Determination of the effective thermoelastic properties of cork-based agglomerates

Marco Delucia, Anita Catapano, Marco Montemurro, Jérôme Pailhès

Determination of the effective thermoelastic properties of cork-based agglomerates

Marco Delucia[a], Anita Catapano[b], Marco Montemurro[a,*], Jérôme Pailhès[a]

[a] *Arts et Métiers ParisTech, I2M CNRS UMR 5295, F-33400 Talence, France*
[b] *Bordeaux INP, Université de Bordeaux, I2M CNRS UMR 5295, F-33400 Talence, France*

Abstract

In this paper, a general numerical homogenisation scheme coupled with an efficient modelling strategy for predicting the effective thermoelastic properties of cork-based agglomerates is presented. In order to generate a realistic representation of the geometry and distribution of particles for the representative volume element (RVE) of the agglomerate at the mesoscopic scale, a general parametric model based on the Voronoi's tesselation (VT) has been developed. However, the classical algorithm for VT has been enhanced by adding a full parametrization of the RVE. The grains composing the RVE are generated by considering the full set of design variables involved at this scale, i.e. the material properties of the constitutive phases (grains and matrix) and the main geometric parameters related to the grain (volume fraction, average diameter, geometric and material orientations). Numerical results show that the macroscopic effective thermoelastic properties of the cork-based agglomerate are strongly affected by the previous parameters in perfect agreement with experimental results available in literature.

Keywords: Cork-based composites, Voronoi's tessellation, Homogenisation, Elastic properties, Thermal properties

This is a pre-print of an article published in *Journal of Reinforced Plastics and Composites*.
The final authenticated version is available online at:
https://doi.org/10.1177/0731684419846991

*Corresponding author. Tel.: +33 55 68 45 422, Fax.: +33 54 00 06 964.
Email addresses: anita.catapano@bordeaux-inp.fr (Anita Catapano), marco.montemurro@ensam.eu, marco.montemurro@u-bordeaux.fr (Marco Montemurro)

1. Introduction

The research on high performance materials plays a role of primary importance for many industrial applications. Nowadays, society is aware of environmental issues and themes as sustainability and recyclability are commonly discussed in industry and academia. The general aim is to reduce the environmental impact due to human activities. One of the main objectives is replacing synthetic and non-renewable materials used for specific applications by natural and renewable materials with similar or even better properties. In the last few decades, among natural, renewable and biodegradable materials, cork has attracted the attention of many researchers and companies thanks to its remarkable properties.

Cork is one of the lightest wood with excellent thermal and acoustic insulation capability suitable to be exploited in many existing applications from construction to aerospace field. Cork is extracted from the outer bark of *Quercus Suber L.* and exhibits a honeycomb-like microstructure, as shown in Figs. 1 and 2, composed of closed cells filled with an air-like gas which represents up the 85-90% of the total volume [1].

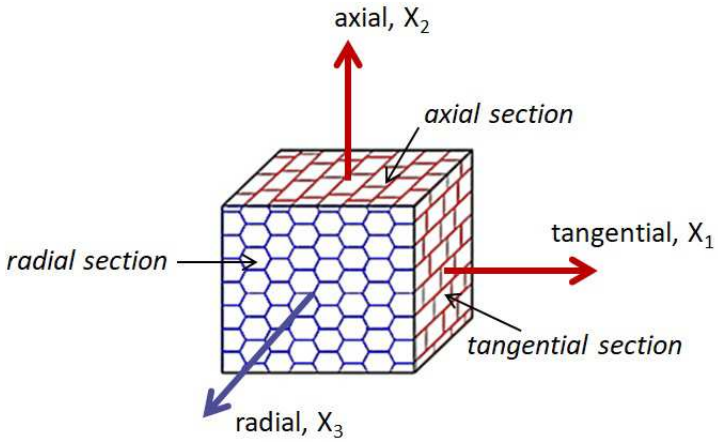

Figure 1: Schematic representation of the honeycomb microstructure and reference frame of cork.

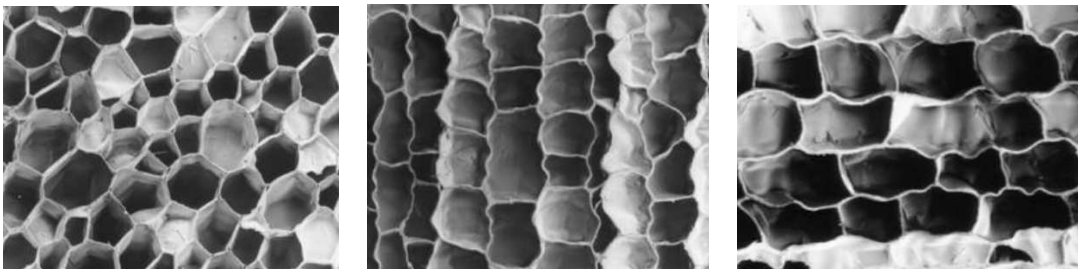

(a) (b) (c)

Figure 2: Structure of the cork observed by scanning electron microscopy: radial (a), axial (b) and tangential section (c), the pictures are taken from [2].

Thanks to its low density, which varies between 120 and 240 kg/m^3, and chemical composition (the suberin and the lignin are the two main components) [3–5], it is a potential candidate for lightweight applications, impermeable to gases and liquids with outstanding acoustic and thermal insulation properties. Furthermore, as a consequence of its viscoelastic behaviour and compressibility, it shows a good damping capability [6, 7]. The mechanical behaviour of cork can be considerd roughly transverse isotropic [6]. The

high variability of density, porosity and chemical composition in the cork planks (which are strongly affected by the geographical location of cork production) explains the natural variability of its macroscopic mechanical properties [3, 8]. In particular, density and porosity are the main parameters influencing the mechanical behaviour of cork. General properties of cork are summarized in Table 1. A review on cork and its application can be found in [1].

Property	**Value**
Density [kg/m^3]	120−180 (amadia) [9]
	160−240 (virgin) [9]
Thermal conductivity [W/mK]	0.045 (cork) [10]
	0.025 (air) [10]
	0.2 (cork cell walls) [10]
Electrical conductivity [S/m]	1.2 x 10^{-10} (25°C) [11]
	1.67 x 10^{-13} (50°C) [11]
Acoustic resistivity [kg/m^{2}s]	1.2 x 10^5 [12]
Specific heat [J/kgK]	350 [10]

Table 1: General properties of cork.

Cork products can be classified in two main categories: natural cork and cork-based agglomerates or composites. The first category does not introduce additional process besides elaboration, cutting and finishing. Instead, cork-based composites are usually obtained by the compression molding process in which a mixture of cork granules and a polymeric binder (polyurethanes resins, phenol-formaldehyde resins, etc.) is compressed in a mould cavity by an hydraulic press (the pressure level depends on the final density sought). After, the mould is placed in an oven at temperatures between 100 and 150°C for a period from one to 20 hours to gurantee a convenient curing stage [1]. Next, the agglomerate is unmoulded and subject to cooling/stabilisation. The result of this process is the cork-based agglomerate in the form of parallelepipedic blocks that subsequently are laminated to get the desired dimensions [1].
Cork-based composites are used in several applications such as, for example, cork stoppers, floor coverings and heat engine seals. They can also be utilised in multilayer plates (e.g. the core of sandwich panels). Cork-based composites exhibit a visco-elasto-plastic behaviour similar to that of the natural cork [1, 13, 14]. The typical compressive stress-strain curve shows a behaviour common to hyper-elastic materials. Generally, for small values of the strain, cells tend to bend elastically through a process fully reversible as illustrated in Fig. 3.
On the other hand, the tensile behaviour of cork-based composites is quite different from the compression one. In particular, a typical tensile stress-strain curve shows a behaviour similar to that of cellular materials [15]. Furthermore, cork-based agglomerates exhibit a thermal insulation capability which is very close to that of the natural cork. In fact, the cellular microstructure of cork, composed of a large amount of air-like gas, allows having an agglomerate with a low thermal conductivity that can be exploited for several applications. An exhaustive review on cork-based composites and their applications can be found in [16].
The thermomechanical properties of cork-based composites depend on the main design and process parameters as the quality, the density, the size and the fraction of cork particles in the mixture, the type and the quantity of polymeric binder, the manufacturing process (pressure and temperature) and the overall packing density [13, 17–22]. For this reason,

there are no general properties for cork-based composites. The main properties of some cork-based agglomerates available in literature are reported in Table 2.

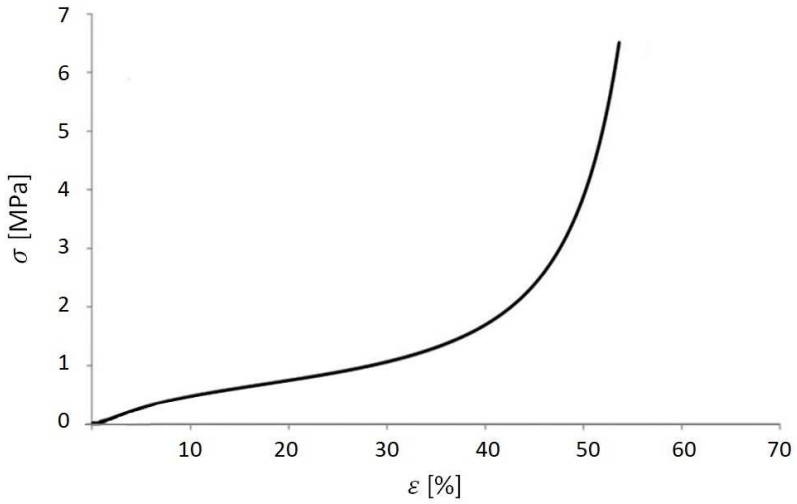

Figure 3: Stress-strain curve in compression for the cork-based composite AC216 [13].

Property	[13]	[13]	[23]	[14]
Density [kg/m^3]	157	216	272	580
Range of grain [mm]	2-4	2-4	small grains	1-3
Binder	Polyurethane	Polyurethane	Epoxy	Epoxy
Binder volume fraction	N/A	N/A	N/A	35
Young's modulus [MPa]	4	6	N/A	180
Thermal conductivity [W/mK]	N/A	N/A	0.047	N/A

Table 2: Properties of some cork-based composites available in literature.

Some studies have been conducted to experimentally investigate the influence of the main design parameters on the properties of cork-based composites.
Jardin *et al.* [13] have shown, by testing different types of cork-based composites, that the overall density, the grain size and the binder type have a clear influence on the mechanical behaviour of the composite. In particular, the higher the relative density of the agglomerate the higher the Young′s modulus.
Castro *et al.* [23] studied the opportunity to exploit cork-based composites as a core material for sandwich components. Bending tests on different core materials, like synthetic foams, commercial cork-based agglomerates and cork-epoxy agglomerates, have shown that by adjusting parameters such as the cork grains average size, type of resin and density, it is possible to control performances of the sandwich components depending on the considered application. In particular, cork-epoxy agglomerates, compared with other core materials, are characterised by a higher shear stress limit. Thermal conductivity tests have revealed that cork-epoxy agglomerates show good thermal insulation properties, similar to synthetic foams. Moreover, the lower the relative density the lower the thermal conductivity of the agglomerate.
Santos *et al.* [21, 22] have designed, produced, tested and compared different cork-based composites in order to obtain a suitable combination of thermal and mechanical properties. In particular, they compared composites with same density, type and percentage

of binder but different grain size in order to assess the influence of this last parameter. Results show that it is possible to tailor mechanical properties by changing design parameters, e.g. the type of binder, in order to delay the densification stage or to have a larger plateau with higher deformations. Furthermore, experimental results concerning thermal conductivity and specific heat show that the thermal behaviour of cork-based composites is not considerably influenced by some parameters as the grain size, room temperature, type and the percentage of resin. Conversely, density of cork-based composites strongly affects their thermal properties.

As it clearly appears from this non-exhaustive literature survey (and also to the best of the authors' knowledge), the influence of the main design and process parameters of cork-based composites on their macroscopic behaviour is often evaluated through experimental tests. In this background, no systematic approach which aims at studying the influence of the full set of the main design and process parameters involved at different scales on the macroscopic thermal and elastic behaviours of cork-based agglomerates has been proposed yet. The aim of the present work is to propose a general (and efficient) multi-scale numerical homogenisation procedure capable of determining the effective (or apparent) thermal and elastic properties of cork-based agglomerates. The goal is the determination of the equivalent macroscopic behaviour of the cork-based composite starting from the behaviour and arrangement of its constituents in order to replace the real heterogeneous material with a fictitious homogeneous medium.

The strategy proposed in this work is focused on the transition from mesoscopic scale to the macroscopic one. The macroscopic thermal and elastic behaviours depend upon different parameters defining the representative volume element (RVE) of the agglomerate: grain orientation, grain shape, grain anisotropy, matrix material properties and volume fraction as well as the properties of the interface between grains and matrix.

To this purpose, a general finite element (FE) model of the agglomerate RVE integrating all the previous parameters is proposed in this work. The modelling strategy relies, on the one hand, on a generalisation of the Voronoi's tesselation (VT) algorithm [24] and, on the other hand, on the strain energy homogenisation technique of periodic media presented in [25–30]. In particular, as far as the VT algorithm is concerned, two affine transformations (i.e. a homothety followed by a local rotation of each grain) have been added in order to closely reproduce the cork-based composite RVE structure at the mesoscopic scale.

The RVE of the cork-based agglomerate is generated in order to take into account for the randomness of both the grain geometric and material frame orientations. The sensitivity analysis of the thermal and elastic properties to both the matrix volume fraction and the cork particle size variability has been conducted. In addition, the effectiveness of the proposed modelling strategy is proven through a meaningful comparison with experimental data taken from the literature [14]. Furthermore, concerning elastic properties, the degree of anisotropy of the equivalent homogeneous material has been evaluated through the numerical approach presented in [26].

The paper is organized as follows: the description of the problem and of the FE-based homogenisation method are presented in Section 2. The parametric model for the generation of the meso-structure and the related 2D FE model for numerical homogenisation are illustrated in Section 3. The sensitivity analysis is detailed in Section 4. The comparison between numerical and experimental results is presented in Section 5. Finally, Section 6 ends the paper with some conclusions and perspectives.

2. Homogenisation of mechanical and thermal properties

Several analytical, experimental and numerical methods can be found in literature for the prediction of elastic and thermal properties of heterogeneous materials, each one showing a different level of sophistication.
Analytical models are often based on simplifying assumptions hypotheses and semi-empirical equations. For instance, the Einstein's equations [31, 32] predict the Young's modulus of particulate-polymers composites using a linear function of the particle volume fraction (V_p) without considering the effect of the inclusions size and the interaction between the matrix and the particles. In order to improve the estimation of the Young's modulus, more elaborated theories have been developed [33–36]. Among analytical theories for homogenisation of elastic properties of composites, the Reuss-Voigt's Lower (RV-LB) and Upper (RV-UB) Bounds [37, 38] and the Hashin-Shtrikman Lower (HS-LB) and Upper (HS-UB) Bounds [39] have been developed to determine a range of existence of the elastic moduli, rather than a single value. Successively, these models have been adapted for determining also the thermal conductivity of composites [40]. However, the previous models can predict only the influence of the material properties of the constitutive phases and of the inclusions volume fraction on the final macroscopic behaviour of the composite, without integrating the effect of other relevant variables like the shape of the inclusions.
More sophisticated models and theories like the Eshelby's model [41], the Mori-Tanaka model [42], the Self-Consistent Scheme [43] and the Lielens' model [44, 45] are able to take into account for the influence of the shape of the particles on the macroscopic behaviour of the composite. Many analytical models have been also developed for the prediction of thermal expansion coefficients of composites, each of one with a different degree of complexity as the model of Schapery (SC) [46], Chamberlain (CB) [47], Chamis (CH) [48], Rosen and Hashin (RH) [49]. However, all these analytical models are characterised by a common strong limitation: the effect of localised fields (stress, strain or temperature) on the macroscopic behaviour is not taken into account.
In order to go beyond the limitations of the analytical models, numerical homogenisation techniques have been developed. FE-based models are very general and, depending on the degree of refinement of the model, they can lead to more realistic solutions. Furthermore, they can be a valid support for experimental tests. Indeed, numerical results can orient the types of experimental tests to be conducted and inversely, the experimental results can validate the numerical model, thus reducing the number of tests, with a consequent reduction of time and costs.
In this work, a general FE model of the cork-based composite RVE is developed. The aim of the proposed modelling strategy is to closely reproduce the real meso-structure of the agglomerate. Therefore, a suitable parametric FE model integrating the main features of the cork-based composite has been conceived. In particular, the FE model of the RVE has been parametrised in terms of the particles shape and size, particles (random) orientation, particles arrangement within the matrix and particles anisotropy as well. It is noteworthy that cork-based composites show a highly random meso-structure, especially in terms of the geometrical arrangement of the particles as well as their shape and orientations (both geometrical and material). Therefore, cork-based composites do not show a periodic meso-structure. In this work the homogenisation method is applied on a RVE sufficiently large in order to be representative of the macroscopic behaviour of the real composite. Moreover, no hypotheses are made on the type of elastic symmetry of the resulting homogenised material. Indeed, the kind and degree of elastic symmetry (e.g. isotropic, cubic, etc.) will be determined analysing, at a later stage, the components of the stiffness tensor of the homogenised material.

The homogenisation procedure is applied to a 2D FE model of the agglomerate RVE under plane strain assumption. In this framework, the effective elastic and thermal properties of the cork-based composite are determined under the following hypotheses:

- linear elastic and thermal behaviours for the material of the constitutive phases;
- perfect bonding for the wall-to-wall contact between matrix and particles.

2.1. Finite element-based homogenisation of elastic properties

The effective properties of the cork-based composite are determined using the strain energy homogenisation technique of periodic media [25, 26]. This method is based on the assumption that both the RVE of the periodic heterogeneous structure and the corresponding volume of the equivalent homogeneous medium undergo the same deformation having, hence, the same strain energy.
Using Voigt's notation, for plane strain hypothesis (ε_z=ε_r=ε_q=0), the generalised Hooke's law of the homogeneous medium is:

$$\begin{Bmatrix} \bar{\varepsilon}_x \\ \bar{\varepsilon}_y \\ \bar{\varepsilon}_s \end{Bmatrix} = \begin{bmatrix} B_{xx} & B_{yx} & B_{xs} \\ B_{yx} & B_{yy} & B_{ys} \\ B_{sx} & B_{sy} & B_{ss} \end{bmatrix} \begin{Bmatrix} \bar{\sigma}_x \\ \bar{\sigma}_y \\ \bar{\sigma}_s \end{Bmatrix} \quad , \tag{1}$$

where $\bar{\varepsilon}$ and $\bar{\sigma}$ are, respectively, the strain and stress vectors referred to the equivalent continuum after homogenisation of the RVE. The components of the compliance matrix $\mathbf{B}$ are expressed under the plane strain field assumption [50].

The converse relation of Eq.(1) is:

$$\begin{Bmatrix} \bar{\sigma}_x \\ \bar{\sigma}_y \\ \bar{\sigma}_s \end{Bmatrix} = \begin{bmatrix} Q_{xx} & Q_{xy} & Q_{xs} \\ Q_{yx} & Q_{yy} & Q_{ys} \\ Q_{sx} & Q_{sy} & Q_{ss} \end{bmatrix} \begin{Bmatrix} \bar{\varepsilon}_x \\ \bar{\varepsilon}_y \\ \bar{\varepsilon}_s \end{Bmatrix} \quad , \tag{2}$$

where $\mathbf{Q}$ is the in-plane stiffness matrix under plane strain assumption, with $\mathbf{B} = \mathbf{Q}^{-1}$. In order to determine the in-plane stiffness matrix of the homogeneous material at the upper scale, a set of periodic boundary conditions (PBCs) must be applied to the RVE. This can be achieved by imposing suitable constraint equations (CEs) on each couple of homologous nodes belonging to the opposite faces of the RVE.
Consider a square RVE of side L, as illustrated in Fig. 4: the set of PBCs can be expressed as

$$\begin{aligned} \mathbf{u}(0,y) - \mathbf{u}(L,y) &= u_x \mathbf{e}_x \quad , \\ \mathbf{u}(x,0) - \mathbf{u}(x,L) &= u_y \mathbf{e}_y \quad , \end{aligned} \tag{3}$$

where $\mathbf{u}$ is the displacement field, while $\mathbf{e}_x$ and $\mathbf{e}_y$ are the unit vectors along x and y axes, respectively. u_x and u_y are arbitrary displacements imposed on the RVE.

Therefore, the components of matrix $\mathbf{Q}$ can be determined column-wise by applying the arbitrary displacements listed in Table 3. These boundary conditions (BCs) correspond to three static analyses wherein the strain tensor is characterised by only one component at time different from zero.

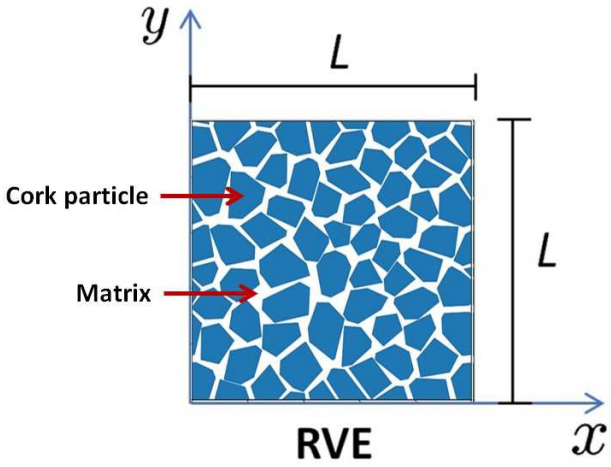

Figure 4: Reference frame of the RVE.

1st load case	2nd load case	3rd load case
$u_x = U_x$	$u_x = 0$	$u_x = U_x/2$
$u_y = 0$	$u_y = U_y$	$u_y = U_y/2$

Table 3: Boundary conditions for the FE model of the RVE.

The components of $\mathbf{Q}$ can be determined from the average strain and stress fields inside the RVE due to the application of PBCs:

$$Q_{\alpha\beta} = \frac{\bar{\sigma}_\alpha}{\bar{\varepsilon}_\beta}, \qquad \text{with } \alpha, \beta = x, y, s \text{ and } \varepsilon_\gamma = 0, \text{ with } \gamma = x, y, s \quad , \quad \gamma \neq \beta \quad . \tag{4}$$

In the previous equation the average stress field is computed as

$$\overline{\sigma}_\alpha = \frac{1}{A_{\text{RVE}}} \int_{A_{\text{RVE}}} \sigma_\alpha(x, y)\, dA \quad , \quad \alpha = x, y, s \quad , \tag{5}$$

whilst the average strain components can be expressed as

$$\bar{\varepsilon}_x = \frac{U_x}{L}, \quad \bar{\varepsilon}_y = \frac{U_y}{L}, \quad \bar{\varepsilon}_s = \frac{U_x + U_y}{L} \quad , \tag{6}$$

where U_x and U_y are the displacements listed in Table 3.

The flow chart of the numerical homogenisation procedure adopted in this work is illustrated in Fig. 5. The entire computational procedure is driven by a Python script interfaced with the FE model built into the ANSYS environment. The user sets the input data concerning the composition of the cork-based composite (i.e. particle average size, particles volume fraction, etc.) as well as the mechanical and thermal properties of its components (elastic constants, density, thermal conductivity and expansion coefficients). Once the RVE geometry is generated in Python, all of the geometric and material data are passed to the ANSYS code in order to build the FE-model of the RVE and run the

numerical homogenisation analyses. The results are then post-processed in Python.

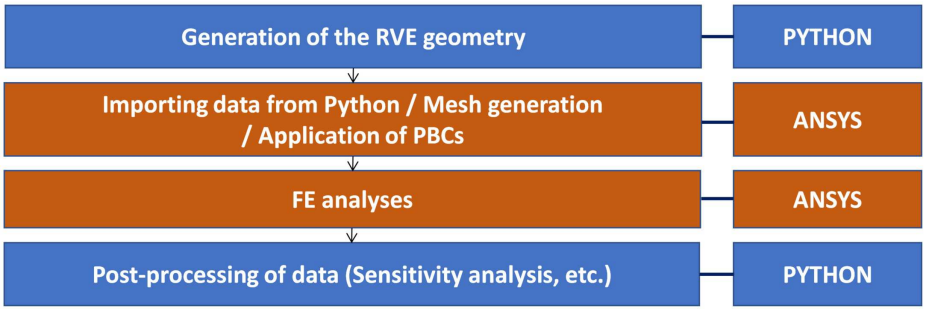

Figure 5: Flow-chart of the numerical homogenisation procedure.

2.2. Finite element-based homogenisation of thermal properties

Analogously to the strain energy homogenisation technique, also effective thermal conductivity and expansion coefficients can be evaluated throught numerical approaches based on the FE method [51, 52].
Concerning thermal conductivity coefficients of the composite, once the FE model of the RVE is generated, the following PBCs must be applied to the opposite faces of the FE model:

$$T\left(x,0\right)-T\left(x,L\right)=\nabla T\cdot\mathbf{e}_{x}L\quad,\quad T\left(0,y\right)-T\left(L,\right)=\nabla T\cdot\mathbf{e}_{y}L\quad, \tag{7}$$

where ∇T represents the arbitrary temperature gradient to be imposed to the RVE.

Then, two steady state thermal analyses are performed on the FE model, by considering the BCs listed in Table 4.

1st load case	**2nd load case**
$\nabla T=\left(\dfrac{\Delta T}{L},0\right)$	$\nabla T=\left(0,\dfrac{\Delta T}{L}\right)$

Table 4: Thermal BCs for the FE model of the RVE.

Once the steady state thermal analyses are solved, the components of the average heat flux per unit line can be determined as:

$$\overline{q}_{\alpha}=\frac{1}{A_{\mathrm{RVE}}}\int_{A_{\mathrm{RVE}}}q_{\alpha}(x,y)\,dA,\ \ \alpha=x,y\quad. \tag{8}$$

The effective thermal conductivity tensor components $K_{\alpha\beta}$ can be calculated column-wise (tensor notation) as follows:

$$K_{\alpha\beta}=\frac{\overline{q}_{\alpha}}{\nabla T\cdot\mathbf{e}_{\beta}}\quad,\ \text{with}\ \alpha,\beta=x,y\quad. \tag{9}$$

The effective coefficients of thermal expansion (CTEs) can be evaluated through two different methods. In the first one (ME1) [53], only a static analysis is necessary. A uniform temperature field ΔT is applied to the entire RVE together with the following BCs (as illustrated in Fig. 6):

$$\begin{aligned} \mathbf{u}(x,0)\cdot\mathbf{e}_y &= 0 \quad , \\ \mathbf{u}(0,y)\cdot\mathbf{e}_x &= 0 \quad , \\ (\mathbf{u}(0,y)-\mathbf{u}(L,y))\cdot\mathbf{e}_y &= 0 \quad , \\ (\mathbf{u}(x,0)-\mathbf{u}(x,L))\cdot\mathbf{e}_x &= 0 \quad . \end{aligned} \tag{10}$$

The previous BCs are imposed in order to obtain a pure extension deformation of the RVE. Then, the effective CTEs α_{ij} (tensor notation) can be calculated as follows:

$$\alpha_{ij} = \frac{1}{\Delta T}\overline{\varepsilon}_{ij} \quad , \qquad \text{with } \; i = x, y \quad . \tag{11}$$

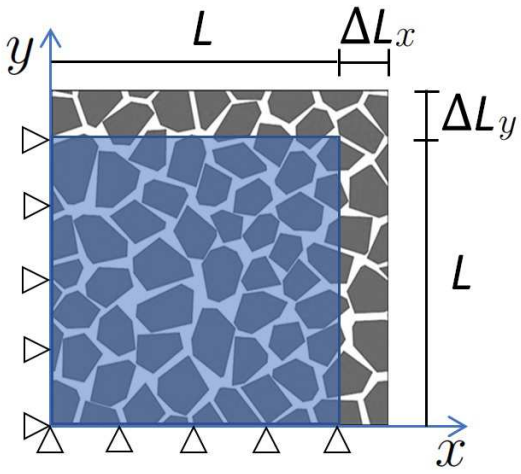

Figure 6: RVE BCs and deformation due to thermal expansion, ME1.

In the second method (ME2) [52], a uniform temperature field ΔT=1°C is applied to the entire FE model along with the following PBCs:

$$\begin{aligned} \mathbf{u}(0,y)-\mathbf{u}(L,y) &= \mathbf{0} \quad , \\ \mathbf{u}(x,0)-\mathbf{u}(x,L) &= \mathbf{0} \quad . \end{aligned} \tag{12}$$

The PBCs of Eq.(12) generate a total strain field equal to zero. Therefore, using the Duhamel-Neumann thermo-elastic law, the equivalent CTEs of the resulting homogeneous medium can be expressed as follows (Voigt's Notation):

$$\alpha_i = -\frac{1}{\Delta T}B_{ij}\bar{\sigma}_j \quad , \quad \text{with } \; i, j = x, y, s \quad . \tag{13}$$

3. Semi-realistic FE models for numerical homogenisation

The FE model has been built using an ad-hoc computational procedure that corresponds to the "generation of the structure at the mesoscopic scale" step of the flowchart presented in Fig. 5. In order to obtain a semi-realistic meso-structure of the cork-based composite, some aspects of fundamental importance needs to be considered. The first aspect is the variable polygonal shape of cork particles that show multiples facets and sharp angles. Moreover, cork particles exhibit transversely isotropic mechanical behaviour, whose material and geometrical frames are randomly oriented within the meso-structure. All these points have been integrated in the algorithm coded in Python environment which aims at generating a meso-structure of the cork-based agglomerate close enough to the real one.

3.1. Generation of the meso-structure: parametric model

The parametric model of the agglomerate meso-structure essentially relies on the VT algorithm. The choice of the VT for representing the geometry of the meso-structure is the most natural one when looking at the true structure of the cork-based composite shown in Fig. 7.

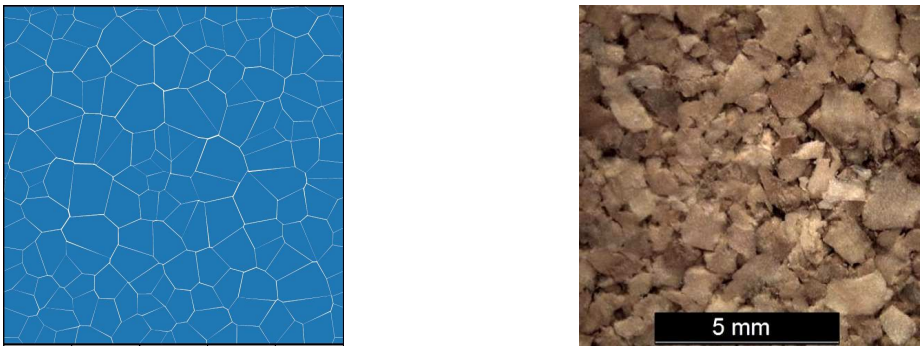

(a) (b)

Figure 7: The parametric model (a) and an image of a cork-based composite (b) taken from [13].

By properly calibrating the parameters of the VT algorithm, it is possible to obtain different configurations of the meso-structure. However, as it can be seen from Fig. 7b, the cork particles are not always arranged according to the Voronoi's configuration but sometimes they are overlapped. Moreover, cork particles show a transverse isotropic elastic behaviour which must be taken into account along with their random arrangement within the agglomerate. All of these aspects are of paramount importance to obtain a semi-realistic meso-structure of the agglomerate. Therefore, classical VT algorithm has been extended by implementing the following features.

3.1.1. Random geometric orientation of cork particles

Polygons generated through the VT are rotated around their center of mass by a random angle to obtain particles without parallel adjacent facets. As shown in Fig. 8, the rotation of polygons is carried out through the algorithm described here below.

Algorithm 1 Polygons random rotation.

1: Exclude the polygons whose edges belong to the RVE boundary.
2: Evaluate the number of remaining polygons N_p. Initialise the slack variable $k = 1$ and set its upper bound to N_p.
3: Set $\lambda \in [0.5, 0.99]$. Select the polygon k and rotate it by a random angle $\theta \in [0°, 359°]$.
4: Build the set of the ID of polygons adjacent to polygon k, i.e. $S_k = (i_1, ..., i_{n_k})$. Let n_k be the total number of polygons belonging to S_k. Set the slack variable $j = 1$.
5: Check intersection between polygons k and i_j. If intersection occurs go to point 6, otherwise go to point 7.
6: $\theta \leftarrow \lambda\theta$ and go to point 5.
7: $j = j + 1$. If $j < n_k$ go to point 5, otherwise continue.
8: The initial polygon is replaced by the rotated one.
9: $k = k + 1$. If $k < N_p$ go to point 3, otherwise continue.
10: Generate the RVE with rotated polygons.

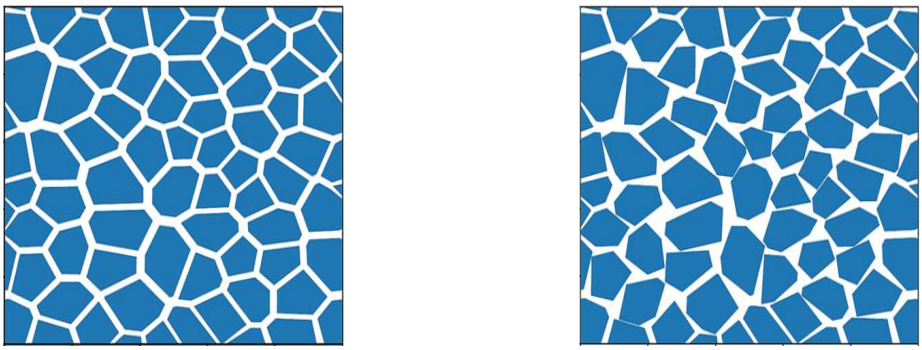

(a) (b)

Figure 8: RVE with parallel-faced particles (a) and with the geometric rotation of particles (b).

3.1.2. Random material frame orientation of cork

Cork has an anisotropic mechanical behaviour and it can be considered roughly as a transversely isotropic material, as discussed in [6], where average values of the elastic moduli were evaluated on different cork specimens, as reported in Table 6 (the elastic properties were evaluated according to the frame illustrated in Fig. 1). Technical elastic constants E_{ci}, G_{cij} and ν_{cij} (with i,j = 1,2,3) are, respectively, the Young's moduli, the shear moduli and the Poisson's ratios of cork in the reference frame {0; x_1, x_2, x_3}.
In order to take into account the random orientation of the material frame of each particle of cork, with respect to the global frame {0; x, y, z} of the 2D mesoscale FE model, an arbitrary 3D rotation of the material frame is applied. For a transversely isotropic material, the 3D stiffness matrix **C** can be written as follows:

$$[C] = \begin{bmatrix} \frac{1-\nu_{c13}\nu_{c31}}{E_{c1}E_{c3}\Delta} & \frac{\nu_{c21}+\nu_{c13}\nu_{c31}}{E_{c1}E_{c3}\Delta} & \frac{\nu_{c31}+\nu_{c21}\nu_{c31}}{E_{c1}E_{c3}\Delta} & 0 & 0 & 0 \\ \frac{\nu_{c21}+\nu_{c13}\nu_{c31}}{E_{c1}E_{c3}\Delta} & \frac{1-\nu_{c13}\nu_{31}}{E_{c1}E_{c3}\Delta} & \frac{\nu_{c31}+\nu_{c12}\nu_{c31}}{E_{c1}E_{c3}\Delta} & 0 & 0 & 0 \\ \frac{\nu_{c31}+\nu_{c21}\nu_{c31}}{E_{c1}E_{c3}\Delta} & \frac{\nu_{c31}+\nu_{c12}\nu_{c31}}{E_{c1}E_{c3}\Delta} & \frac{1-\nu_{c12}\nu_{c21}}{{E_1}^2\Delta} & 0 & 0 & 0 \\ 0 & 0 & 0 & G_{c13} & 0 & 0 \\ 0 & 0 & 0 & 0 & G_{c13} & 0 \\ 0 & 0 & 0 & 0 & 0 & \frac{E_{c1}}{2(1+\nu_{c12})} \end{bmatrix}, \quad (14)$$

where

$$\Delta = \frac{1 - (\nu_{c12}\nu_{c21}) - 2(\nu_{c13}\nu_{c31}) - 2(\nu_{c21}\nu_{c31}\nu_{c13})}{(E_{c1}^2 E_{c3})} \quad . \tag{15}$$

The 3D rotation of the material frame is described using Euler's angles ψ, β and γ [54]. The stiffness tensor in the rotated frame is expressed as

$$\left[C'\right] = \left[R\right]\left[C\right]\left[R\right]^T \quad , \tag{16}$$

where R is the rotation matrix described in [55]. The technical elastic constants, to be assigned to a cork particle in the 2D FE model, are the constants get by the matrix $[C']$ in the rotated frame considering only the components in the global reference plane $x - y$ due to the plane strain hypothesis.

3.1.3. Generation of the agglomerate RVE: the algorithm

The flowchart of the algorithm developed for the generation of the agglomerate RVE is shown in Fig. 9. The main steps charactering such an algorithm are described here below.

1. N points are randomly generated within one eight of the overall RVE volume. A minimum distance D_{min} between two points is defined in order to delete and regenerate points placed at a distance lower than D_{min}.
2. The volume generated at the first step is duplicated eight times and translated along six different directions (top, bottom, right, left, and along two main diagonals) in order to ensure the periodicity of points belonging to the RVE boundary.
3. The polygons are created using the VT algorithm.
4. A scaling factor is applied to all the polygons in order to reduce their dimensions and create voids that will be filled by the matrix (resin). The scaling factor is directly related to the matrix volume fraction.
5. Particles are rotated by means of the Algorithm 1. This new feature allows generating a geometrical meso-structure of the RVE which is closer to the real one.
6. The material frame of each particle is randomly turned and the material properties of each particle are defined in this frame.

3.2. The FE model

The FE model of the cork-based composite RVE has been built into the ANSYS® environment. The geometry is parametrised and generated in PYTHON by means of the algorithm presented in the previous section and then passed to the ANSYS environment in order to carry out the required FE analyses.
For the structural static analyses the 6-nodes plane quadratic triangular element PLANE 183, with two degrees of freedom per node has been used. While for the steady-state thermal analysis the 6-node plane quadratic triangular element PLANE 77, with a single degree of freedom, i.e. the temperature, at each node, has been used. Furthermore, for mechanical analyses the plain strain option has been activated.
The model along with its mesh is illustrated in Fig. 10.
In order to derive the equivalent stiffness tensor of the homogeneous material at the macroscopic scale, three static analyses are required with the BCs listed in Table 3. On the other hand, in order to determine the equivalent conductivity tensor only two thermal analyses are performed by using the BCs listed in Table 4. Finally, to evaluate the effective CTEs

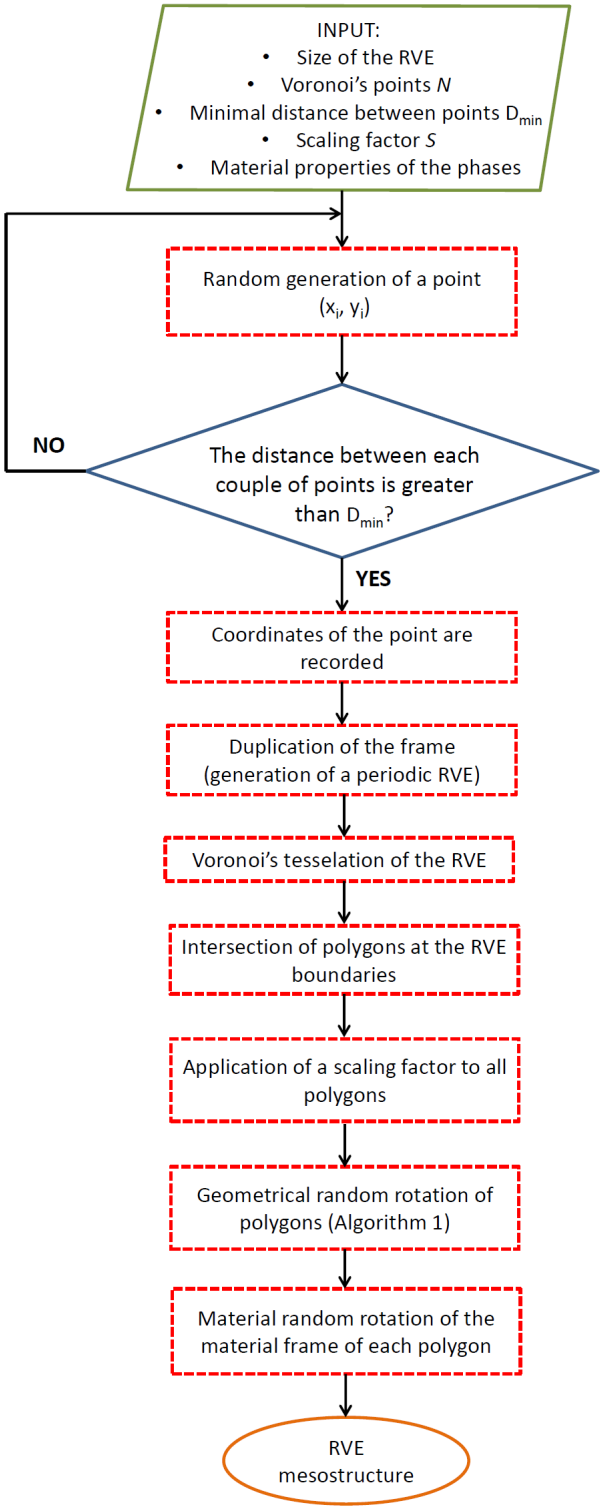

Figure 9: Flowchart of the algorithm to generate the meso-structure of the RVE.

only a single analysis is needed by using either the BCs of Eq. (10) or the PBCs of Eq. (12), for ME1 or ME2, respectively.

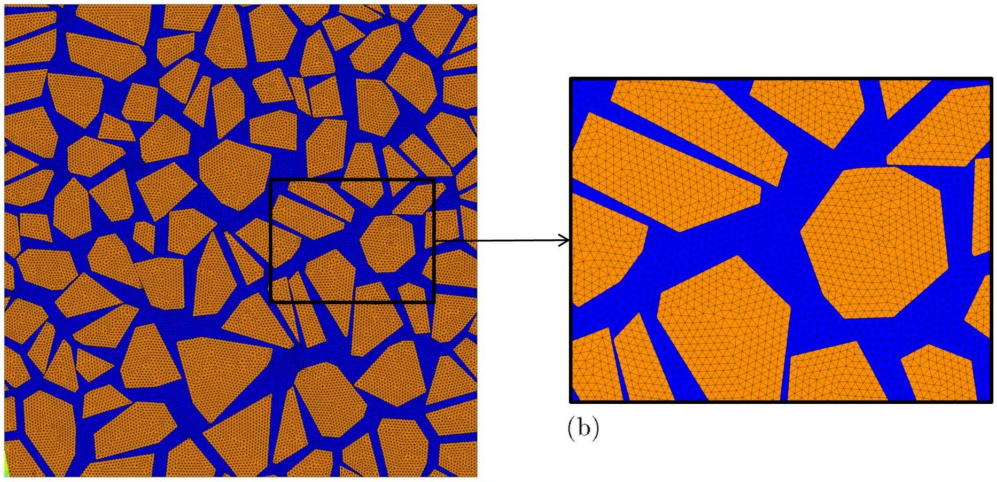

(a) (b)

Figure 10: Finite element model of the RVE (a) and detail of the mesh (b).

4. Numerical study

In this section, a sensitivity analysis of the effective thermomechanical properties of the cork-based agglomerate to the main material and geometrical parameters of the meso-structure has been carried out. In particular, the influence of (a) the material properties of the constitutive phases, (b) the matrix volume fraction, (c) the average size and (d) the geometric and material orientation of the cork particles on the macroscopic thermo-mechanical behaviour is investigated.

4.1. FE-model calibration

Before performing the sensitivity analysis in terms of both geometrical and material parameters of the agglomerate RVE, the effect of the mesh size on the cork-based composite macroscopic behaviour must be analysed. The FE-model calibration has been carried out on a realistic configuration of the agglomerate characterised by the properties listed in Table 5.

Property	**Value**
Mass percentage of cork	84%
Mass percentage of resin	16%
Diameter of the particles	0.5 mm and 1 mm
Particles of 0.5 mm	50%
Particles of 1 mm	50%

Table 5: Properties of the cork-based composites used for the mesh sensitivity analysis.

The material properties of the constitutive phases of the agglomerate, i.e. natural cork and resin, are listed in Table 6. This composition corresponds to a composite with a matrix volume fraction equal to 0.02 calculated using data in Tables 5 and 6.

The sensitivity of the equivalent macroscopic behaviour of the cork-based composite to the mesh size has carried out on three different RVE sizes (10, 90 and 180 mm^2) where only the mesh density (i.e. number of elements per unit area) varies while the rest of the RVE parameters is kept constant. The convergence has been checked by analysing the

Material	Density	Mechanical properties	Thermal properties
Cork	120 [kg/m^3] [14]	$E_{c1} = E_{c2} = 13$ [MPa] [6] $E_{c3} = 20$ [MPa] [6] $G_{c12} = 4.3$ [MPa] [6] $G_{c13} = E_{c23} = 2.5$ [MPa] [6] $\nu_{c12} = 0.5$ [6] $\nu_{c13} = \nu_{c23} = 0$ [6]	$K_c = 0.045$ [W/mK] [5] $\alpha_c = 180$ [$10^{-6}(\mathrm{C}^o)^{-1}$] [56]
Epoxy resin	1100 [kg/m^3] [14]	$E_m = 2810$ [MPa] [14] $\nu_m = 0.39$ [14]	$K_c = 0.35$ [W/mK] [14] $\alpha_c = 55$ [$10^{-6}(\mathrm{C}^o)^{-1}$] [57]

Table 6: Material properties of the cork and the epoxy resin.

numerical values of components Q_{xx}, Q_{yy} and Q_{ss} of the stiffness matrix. For the sake of brevity, only the values of Q_{xx} versus the mesh density for a RVE size of 10 mm^2 are illustrated in Fig. 11. The curves relative to the other two components Q_{yy} and Q_{ss} of the stiffness matrix lead to the same conclusions given by Fig. 11. The convergence of elastic properties is achieved for a value of the mesh density equal to 2779 mm^{-2}.
The second aim of the FE-model calibration phase is the identification of the smaller size of the RVE capable to properly represent the macroscopic behaviour of the composite material. Seventeen values of the RVE size have been analysed and for each one of them, ten different meso-structures have been generated, using a mesh density equal to 2779 mm^{-2}. For this second type of analyses, the matrix volume fraction has been kept equal to 0.02. The values Q_{xx}, Q_{yy} and Q_{ss} of the stiffness matrix have been analysed by focusing on the standard deviation. Adopting a tolerance interval not greater than 1% for the standard deviation of each elastic property, the convergence has been achieved for an RVE size equal to 130 mm^2. For the sake of brevity, only the values of Q_{xx} and its standard deviation vs. the RVE size are shown in Fig. 12. The same consideration can be repeated for the other components of the agglomerate stiffness tensor at the macroscopic scale.

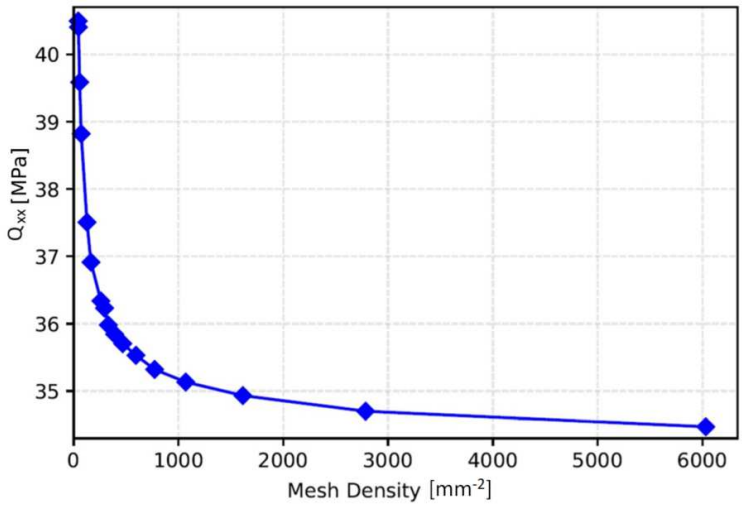

Figure 11: Q_{xx} vs the mesh density for a RVE of 10 mm^2.

4.2. Parametric analysis

Once the FE-model has been calibrated in terms of mesh density and RVE size, a parametric analysis can be performed in order to investigate the influence of the most

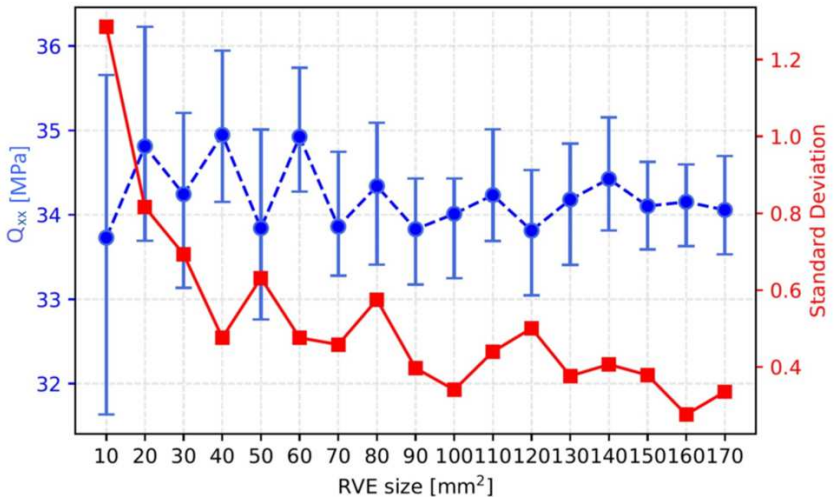

Figure 12: Q_{xx} and its standard deviation vs the RVE size.

relevant geometrical and material parameters of the RVE on the macroscopic thermal and mechanical properties of the cork-based composite. All the analyses have been carried out on RVE configurations characterised by a random geometric orientation and the random material frame orientation of cork particles.
A reference value has been chosen for each design variable and, for each parametric analysis, only one parameter at time is changed as listed in Table 7.

Parameters	Reference value	Interval	Discretisation step
Matrix volume fraction (V_m)	0.02	$0.02 \div 0.10$	0.01
Particle size variability [mm] (C_{var})	0.25	$0.25 \div 0.45$	0.05

Table 7: Reference value, variation interval and discretisation step for each parametric analysis.

The parameter C_{var} is the standard deviation of the average value of all the particles of the RVE represented by circles of equivalent area.
In the first parametric analysis the effect of matrix volume fraction on the macroscopic material properties of the composite has been evaluated. Numerical results have been compared to the analytical models of Reuss-Voigt and of Hashin-Shtrikman.

Furthermore, the degree of elastic symmetry of the resulting composite has been evaluated according to the criterion presented in [26]. In the present work, the components of the stiffness matrix $\mathbf{Q}$ have been compared to determine the degree of elastic symmetry of the cork-based composite. In fact, for an isotropic material, the stiffness matrix $\mathbf{Q}$ in terms of homogenised Young's modulus and Poisson's ratio is:

$$Q = \frac{E}{(1+\nu)(1-2\nu)} \begin{bmatrix} 1-\nu & \nu & 0 \\ \nu & 1-\nu & 0 \\ 0 & 0 & 2(1-2\nu) \end{bmatrix}. \tag{17}$$

Therefore, for an isotropic material the ratios Q_{yy}/Q_{xx} and $Q_{ss}/((Q_{xx}-Q_{xy})/2)$ are equal to one, while the ratios Q_{xs}/Q_{xx} and Q_{ys}/Q_{xx} are equal to zero. Assuming a

tolerance interval of ± 0.05, the cork-based composite exhibits a cubic behaviour in all numerical results related to the first parametric analysis, as shown in Fig. 13. Accordingly, the composite material is characterised, at the macroscopic scale, by three independent elastic constants. Indeed, in the case of cubic symmetry the shear modulus does not depend upon the Young's modulus and the Poisson's ratio.

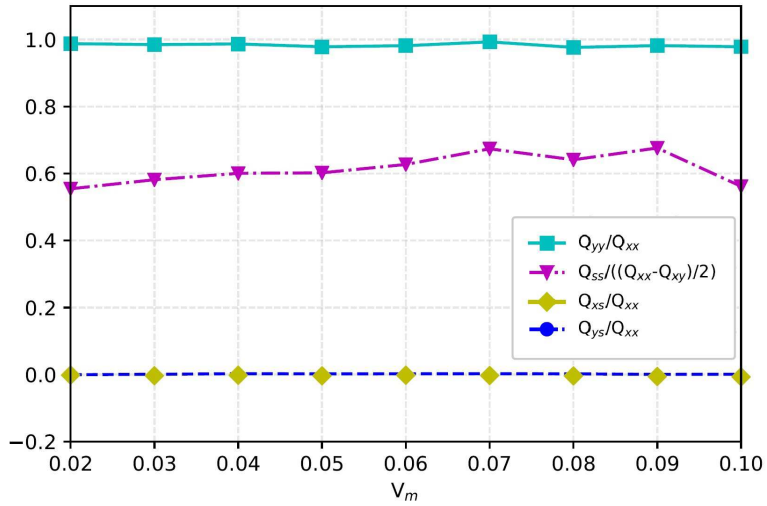

Figure 13: Ratios Q_{yy}/Q_{xx}, $Q_{ss}/((Q_{xx} - Q_{xy})/2)$, Q_{xs}/Q_{xx} and Q_{ys}/Q_{xx} vs the matrix volume fraction V_m.

The Young's modulus and the shear modulus of the cork-based composites as function of the matrix volume fraction are shown in Figs. 14 and 15 respectively. Of course, since the matrix is stiffer than the cork, the greater the matrix volume fraction the higher the stiffness of the agglomerate.
Equivalent elastic properties fall within lower and upper bounds of Reuss-Voigt (i.e. RV-LB and RV-UB, respectively) and of Hashin-Shtrikman (i.e. HS-LB and HS-UB, respectively). More precisely, the numerical results are closer to the lower bounds.

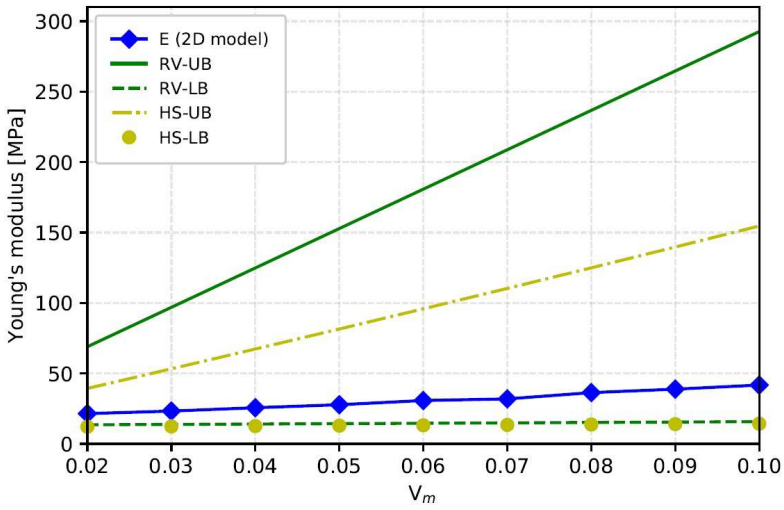

Figure 14: Young's modulus vs the matrix volume fraction V_m.

The equivalent Poisson's ratio falls within RV and HS bounds and it is closer to the upper bounds for high values of the matrix volume fraction, as shown in Fig. 16.

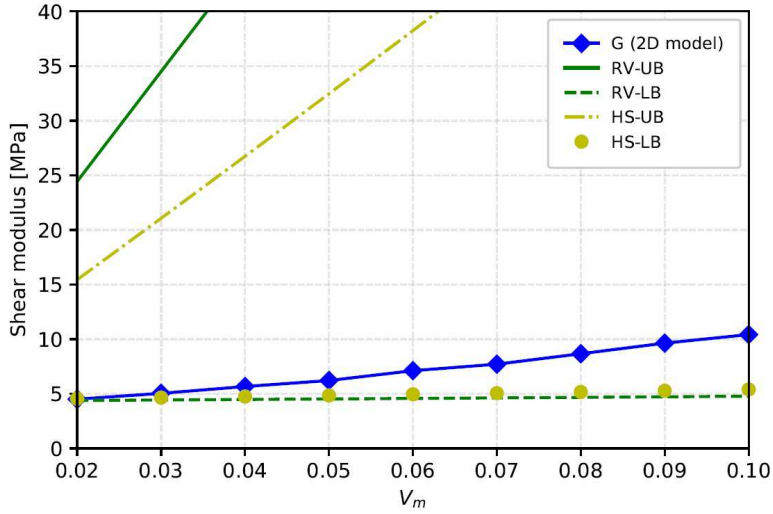

Figure 15: Shear modulus vs the matrix volume fraction V_m.

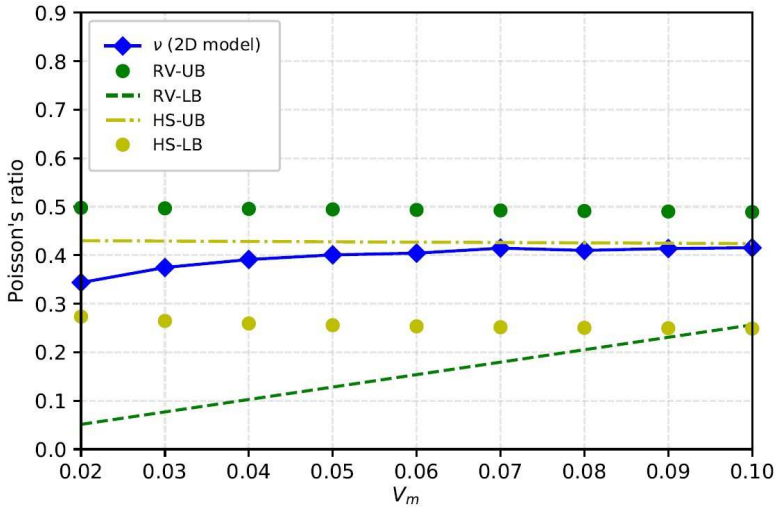

Figure 16: Poisson's ratio vs the matrix volume fraction V_m.

The variation of the effective thermal conductivity coefficients vs. the matrix volume fraction V_m is presented in Fig. 17. Numerical results show that effective thermal conductivity increases when the matrix volume fraction increases. Also in this case, numerical results have been compared to analytical ones.

Finally, the variation of the composite CTEs vs. the V_m has been analysed. The results reported in Table 8 summarise the variation of the effective CTEs, evaluated by means of both the analytical models SC [46] and CH [48] and the numerical models ME1 and ME2, vs. the matrix volume fraction. Both SC and CH models allows determining the longitudinal and transverse CTEs (i.e. α_x and α_y, respectively) of fibres-reinforced composites. The SC model considers an isotropic behaviour for both matrix and fibres, while the CH model takes into account for the transversely isotropic behaviour of the fibre. Therefore, for the case of particle-reinforced composites as cork-based agglomerates, the analytical results calculated with SC and CH models can be considered as bounds. The percentage difference (PD) between the CTEs obtained using ME1 and ME2 techniques is also reported in Table 8. It can be noticed that the maximum percentage difference

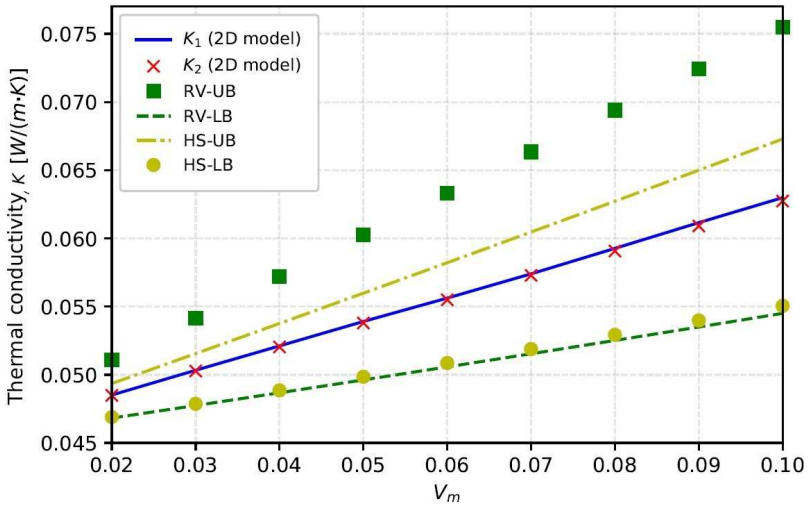

Figure 17: Thermal conductivity coefficient k vs the matrix volume fraction V_m.

between the results given by the two methods is equal to 2.55%. Moreover, concerning the trend of the CTEs, it can be observed that the grater V_m the lower α_x and α_y.

	α_x and α_y $[10^{-6}(\mathrm{C}^o)^{-1}]$					
V_m	SC, CH (α_x)	SC (α_y)	CH (α_y)	ME1 (α_x, α_y)	ME2 (α_x, α_y)	PD^* (α_x, α_y)
0.02	87.32	177.25	178.80	123.08, 125.41	121.31, 123.61	1.45, 1.45
0.03	78.38	175.98	178.17	115.02, 113,59	112.70, 111.46	2.04, 1.89
0.04	73.24	174.71	177.53	106.53, 106.42	104.02, 104.05	2.38, 2.25
0.05	69.89	173.46	176.90	101.30, 102.82	98.78, 100.64	2.52, 2.14
0.06	67.54	172.20	176.26	99.08, 98.60	96.76, 96.31	2.37, 2.35
0.07	65.80	170.96	175.61	94.34, 97.21	92.01, 95.13	2.50, 2.16
0.08	64.46	169.70	174.96	92.78, 94.13	90.44, 92.23	2.55, 2.04
0.09	63.39	168.45	174.31	92.38, 91.97	90.34, 90.05	2.23, 2.11
0.10	62.53	167.21	173.65	91.87, 89.46	89.75, 87.55	2.33, 2.16

* Percentage Difference between the numerical results of ME1 and ME2.

Table 8: CTEs vs the matrix volume fraction V_m.

In the second parametric analysis, five configurations of the RVE with a different particle size variability C_{var} have been analysed. The elastic constants of the composite are presented in Table 9: in agreement with experimental tests presented in [14], the greater the variability in the size of cork grains the higher the stiffness of the agglomerate. Furthermore, as shown in Table 10, also when varying the particle size variability, the cork-based composite exhibits a cubic behaviour. In particular, the cubic behaviour seems to be more pronounced when increasing the particle size variability.

	C_{var} [mm]				
Effective elastic moduli	0.25	0.30	0.35	0.40	0.45
E [MPa] (2D model)	21.4658	21.7246	22.1801	22.6906	22.8395
G [MPa] (2D model)	4.5053	4.7293	4.9041	5.1929	5.2382
ν (2D model)	0.3436	0.3392	0.3351	0.3325	0.3276

Table 9: Elastic moduli vs the cork particle size variability C_{var}.

	C_{var} [mm]				
Ratio	0.25	0.30	0.35	0.40	0.45
Q_{yy}/Q_{xx}	0.987	0.9865	0.9864	0.9865	0.9862
$Q_{ss}/((Q_{xx}-Q_{xy})/2)$	0.5542	0.5748	0.5893	0.6003	0.6149
Q_{xs}/Q_{xx}	-0.0004	-0.0028	-0.0051	-0.0061	-0.0063
Q_{ys}/Q_{xx}	-0.0016	0.0002	0.0018	0.0031	0.0034

Table 10: Ratios Q_{yy}/Q_{xx}, $Q_{ss}/((Q_{xx}-Q_{xy})/2)$, Q_{xs}/Q_{xx} and Q_{ys}/Q_{xx} vs the cork particle size variability C_{var}.

5. Case study

To further prove the effectiveness of the proposed modelling strategy, numerical results ar compared to the experimental ones presented in [14]. The cork-based composite tested in [14] is characterised by the composition given in Table 11.

Property	**Value**
Cork volume fraction	0.65
Matrix volume fraction	0.35
Diameter of the particles	1 mm and 3 mm
Particles of 1 mm	50%
Particles of 3 mm	50%

Table 11: Properties of the cork-based composites used for the mesh sensitivity analysis.

In [14], the author used square specimens and conducted a compressive test to determine the Young's modulus. An isotropic epoxy resin with $E = 2810$ MPa and $\nu = 0.39$ has been used as matrix. The elastic properties of the natural cork used for these tests was not specified. Accordingly, data taken from [6] and detailed in Table 6, regarding average values of the mechanical behaviour of cork, have been used.
Firstly, the FE model has been calibrated: the convergence of elastic properties has been found for a mesh density of 2779 mm^{-2} and for a RVE size of 500 mm^2.
In order to verify the effect of the random geometric and material rotation of the particles on the model response, the effective elastic moduli have been evaluated for four different configurations of the FE model.

1. No geometric and material frame rotation of particles.
2. Random geometric rotation of particles activated but not the material frame one.
3. Random material frame rotation of particles activated but not the geometrical one.
4. Both random geometric and material frame rotation of particles activated.

The Young's modulus obtained with the present numerical model for each one of the previous configurations is shown in Table 12. Numerical results of the configuration characterised by a rotation of both geometrical and material frames of the particles are in very good agreement with the experimental ones. This result is a "numerical proof" of the importance of the new features implemented within the classic VT algorithm to model cork-based composites. Moreover, as it can be observed from Table 12, also the Young's modulus evaluated in the second test case (i.e. when only the random geometric rotation of particles is activated) is close enough to the experimental value found in [14]. This phenomenon can be explained by looking at Fig. 18 where a comparison between the Von Mises stress obtained for a uniaxial traction test along the x-direction of the RVE, is given.

In particular Fig. 18a shows the Von Mises stresses obtained on the model corresponding to the third test case (i.e. where only random material frame orientation is active) while Fig. 18b shows the Von Mises stresses generated in the model corresponding to the fourth test case. From Fig. 18a and 18b it can be observed that the stress field is mainly localised into the matrix and it is influenced by the arrangement of cork particles. Unlike the classical VT where particles have parallel sides and the "matrix path" is smooth, when a random geometric rotation of particles is activated, the matrix path between particles is "warped" due to the particle rotation and the stress flow is redistributed between matrix and particles. Since cork particles are less stiff than the matrix, the configuration with the random geometric rotation of particles shows a Young's modulus lower than that characterising a classical Voronoi's arrangement of particles.

Young's modulus	[14]	First case	Second case	Third case	Fourth case
E [MPa]	180	210	170	217	177

Table 12: Young's modulus for the four different configurations of the RVE of the cork-based agglomerate.

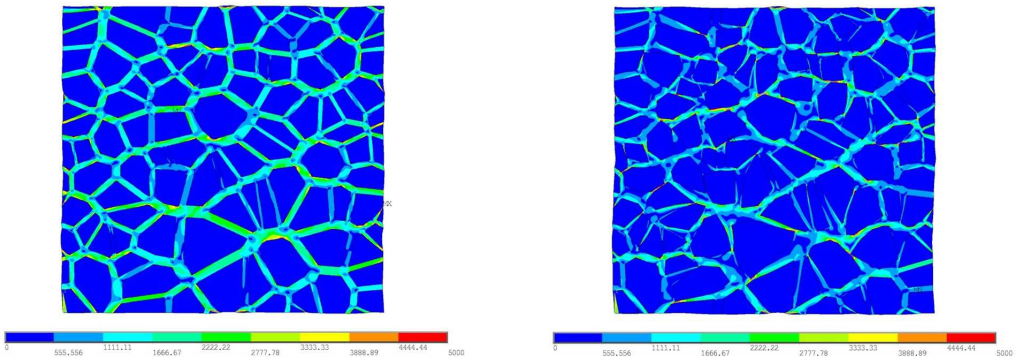

(a) (b)

Figure 18: Von Mises stress in the FE-model of the RVE corresponding to the third test case (a) and to the fourth test case (b), uniaxial traction along x-direction.

6. Conclusions and perspectives

In this work a general numerical model for determining the equivalent thermomechanical properties of cork-based agglomerates has been presented. This model is based, on the one hand, on a general numerical homogenisation scheme, and, on the other hand, on an enhanced version of the VT algorithm. Special attention has been put on the development of a numerical model of the RVE reproducing all the main features of the meso-structure of the composite: random orientation of particles and random orientation of the material frame of each particle as well.

The effectiveness of the proposed modelling strategy has been proven through a large campaign of numerical tests and by means of a comparison with some experimental results taken from literature. In a first time, the calibration of the FE-model of the RVE is performed and then, a parametric homogenisation analysis is carried out. The numerical results highlight that the thermomechanical properties of the cork-based composite are affected, not only by the constitutive phases volume fraction, but also by the variability of the particle size. Moreover, by analysing the components of the stiffness matrix of the

homogenised material, it has been proven that the cork-based composite exhibits a cubic elastic symmetry at the macroscopic scale. Therefore, the shear stiffness modulus is independent from the Young's modulus and the Poisson's ratio. This result is in agreement with those presented in [26] which focuses on the analysis of the degree of symmetry of particle-reinforced composites.
Finally, the results provided by the proposed modelling strategy have been compared to experimental data taken from literature. Results show that, when a random rotation of both the particle and its material frame are taken into account, the numerical results are in excellent agreement with the experimental ones, thus proving the effectiveness of the enhanced version of the VT algorithm.
As far as perspectives of this work are concerned, research is ongoing, on the one hand, on the generalisation of the algorithm for generating a realistic meso-structure of the cork-based agglomerate to the 3D case and, on the other hand, on the integration into the modelling strategy of the following features: the variability of both geometric and material parameters of the RVE, the non-linear thermomechanical behaviour of the material, the influence on the overall macroscopic behaviour of the compression stress field into the particles due to the process (e.g. compression moulding) and the influence of imperfect interfaces between matrix and cork particles.

Acknowledgements

The first author is grateful to the Nouvelle-Aquitaine region, Lièges HPK and SAFRAN Power Units for their contribution to this paper through the LIAMA project.

References

[1] H. Pereira, Cork: Biology, Production and Uses, 2007. doi:10.1016/B978-0-444-52967-1.X5000-6.

[2] H. Pereira, The rationale behind cork properties: A review of structure and chemistry, BioResources 10 (3) (2015) 1–23. doi:10.15376/biores.10.3.Pereira.

[3] H. Pereira, Chemical composition and variability of cork from Quercus suber L., Wood Science and Technology 22 (3) (1988) 211–218. doi:10.1007/BF00386015.

[4] A. J. C. Arteiro, State-of-the-art: Sandwich Structures Applications in Impact Situations, Research Initiation Scolarship Report, Tech. rep., Department of Mechanical Engineering, Faculty of Engineering, University of Porto (2010).

[5] S. P. Silva, M. A. Sabino, E. M. Fernandes, V. M. Correlo, L. F. Boesel, R. L. Reis, Cork: properties, capabilities and applications, International Materials Reviews 53 (4) (2008) 256–256. doi:10.1179/174328008X353529.
URL http://www.tandfonline.com/doi/full/10.1179/174328008X353529

[6] L. J. Gibson, K. E. Easterling, M. F. Ashby, The Structure and Mechanics of Cork, Proceedings of the Royal Society A: Mathematical, Physical and Engineering Sciences 377 (1769) (1981) 99–117. doi:10.1098/rspa.1981.0117.

[7] J. F. Mano, Creep-recovery behaviour of cork, Materials Letters 61 (11-12) (2007) 2473–2477. doi:10.1016/j.matlet.2006.03.157.

[8] V. Oliveira, M. E. Rosa, H. Pereira, Variability of the compression properties of cork, Wood Science and Technology 48 (5) (2014) 937–948. doi:10.1007/s00226-014-0651-2.

[9] M. A. Fortes, M. Emília Rosa, Densidade da cortiça: factores que a influenciam, booktitle = Boletim do Instituto dos Produtos Florestais Cortiça, Vol. 593, 1988, pp. 65–68.

[10] L. Gil, Cortiça: produção, tecnologia e aplicação, INETI, Lisbon, 1998.

[11] M. A. Fortes, M. Teresa Nogueira, Mater. Sci. Eng., Vol. A122, 1989, pp. 272–232.

[12] H. Medeiros, Porquê Isolamentos a Base de Cortiça?, in: Boletim da Junta Nacional de Cortiça, 1945, pp. 165–170.

[13] R. Jardin, F. Fernandes, A. Pereira, R. Alves de Sousa, Static and dynamic mechanical response of different cork agglomerates, Materials & Design 68 (2015) 121–126. doi:10.1016/j.matdes.2014.12.016.
URL http://linkinghub.elsevier.com/retrieve/pii/S0261306914009984

[14] S. Kim, A study on cork-based plastic composite material (2011).

[15] R. A. S. Moreira, F. J. Q. De Melo, J. F. Dias Rodrigues, Static and dynamic characterization of composition cork for sandwich beam cores, Journal of Materials Science 45 (12) (2010) 3350–3366. doi:10.1007/s10853-010-4356-0.

[16] L. Gil, Cork composites: A review (2009). doi:10.3390/ma2030776.

[17] O. Anjos, H. Pereira, M. E. Rosa, Effect of quality, porosity and density on the compression properties of cork, Holz als Roh - und Werkstoff 66 (4) (2008) 295–301. doi:10.1007/s00107-008-0248-2.

[18] O. Anjos, H. Pereira, M. E. Rosa, Tensile properties of cork in the tangential direction: Variation with quality, porosity, density and radial position in the cork plank, Materials and Design 31 (4) (2010) 2085–2090. doi:10.1016/j.matdes.2009.10.048.

[19] O. Anjos, H. Pereira, M. E. Rosa, Characterization of radial bending properties of cork, European Journal of Wood and Wood Products 69 (4) (2011) 557–563. doi:10.1007/s00107-010-0516-9.

[20] O. Anjos, C. Rodrigues, J. Morais, H. Pereira, Effect of density on the compression behaviour of cork, Materials and Design 53 (2014) 1089–1096. doi:10.1016/j.matdes.2013.07.038.

[21] P. T. Santos, S. Pinto, P. A. Marques, A. B. Pereira, R. J. Alves de Sousa, Agglomerated cork: A way to tailor its mechanical properties, Composite Structures 178 (2017) 277–287. doi:10.1016/j.compstruct.2017.07.035.

[22] T. Santos, J. Amaral, V. Costa, V. Amaral, Thermal Conductivity of Agglomerate Cork, in: Materials Research Proceedings, Vol. 3, 2017, pp. 1–10. doi:http://dx.doi.org/10.21741/9781945291418-1.

[23] O. Castro, J. M. Silva, T. Devezas, A. Silva, L. Gil, Cork agglomerates as an ideal core material in lightweight structures, Materials and Design 31 (1) (2010) 425–432. doi:10.1016/j.matdes.2009.05.039.

[24] R. Riedinger, M. Habar, P. Oelhafen, H. J. Güntherodt, About the Delaunay-Voronoi tesselation, Journal of Computational Physics 74 (1) (1988) 61–72. doi:10.1016/0021-9991(88)90068-X.

[25] E. J. Barbero, Finite element analysis of composite materials using ansys, 2013.
URL http://books.google.it/books?id=tWx{_}NLLD14wC{&}printsec=frontcover{&}dq=Fini

[26] A. Catapano, J. Jumel, A numerical approach for determining the effective elastic symmetries of particulate-polymer composites, Composites Part B: Engineering 78 (2015) 227–243. doi:10.1016/j.compositesb.2015.03.085.

[27] M. Montemurro, A. Catapano, D. Doroszewski, A multi-scale approach for the simultaneous shape and material optimisation of sandwich panels with cellular core, Composites Part B: Engineering 91 (2016) 458–472. doi:10.1016/j.compositesb.2016.01.030.

[28] T. Gentieu, A. Catapano, J. Jumel, J. Broughton, Computational modelling of particulate-reinforced materials up to high volume fractions: Linear elastic homogenisation, Proceedings of the Institution of Mechanical Engineers, Part L: Journal of Materials: Design and Applicationsdoi:10.1177/1464420717707227.

[29] L. Cappelli, M. Montemurro, F. Dau, L. Guillaumat, Characterisation of composite elastic properties by means of a multi-scale two-level inverse approach, Composite Structures 204 (2018) 767–777. doi:10.1016/j.compstruct.2018.08.007.

[30] K. Refai, M. Montemurro, C. Brugger, N. Santier, Determination of the effective elastic properties of titanium lattice structures, Mechanics of Advanced Materials and Structuresdoi:10.1080/15376494.2018.1536816.

[31] A. Einstein, Über die von der molekularkinetischen Theorie der Wärme geforderte Bewegung von in ruhenden Flüssigkeiten suspendierten Teilchen, Annalen der Physik 322 (8) (1905) 549–560. arXiv:9811186, doi:10.1002/andp.19053220806.

[32] T. A. A. Broadbent, A. Einstein, H. Hertz, H. L. Dryden, F. P. Murnaghan, H. Bateman, Investigations on the Theory of the Brownian Movement, The Mathematical Gazette 41 (337) (1957) 231. arXiv:9811186, doi:10.2307/3609228.
URL http://www.jstor.org/stable/3609228?origin=crossref

[33] E. Guth, Theory of filler reinforcement, Journal of Applied Physics 16 (1) (1945) 20–25. doi:10.1063/1.1707495.

[34] J. C. Halpin, Stiffness and Expansion Estimates for Oriented Short Fiber Composites, Journal of Composite Materials 3 (4) (1969) 732–734. doi:10.1177/002199836900300419.

[35] J. C. Halpin, Effects of Environmental Factors on Composite Materials, Technical Report Afml-Tr-67-423, Wright-Patterson Air Force Base, OH: Air Force Materials Laboratory (1969).

[36] E. H. Kerner, The elastic and Thermo-elastic properties of composite media, Proceedings of the Physical Society. Section B 69 (8) (1956) 808–813. doi:10.1088/0370-1301/69/8/305.

[37] W. Voigt, Ueber die Beziehung zwischen den beiden Elasticitatsconstanten isotroper korper, Annalen der Physik 274 (12) (1889) 573–587. arXiv:arXiv:1011.1669v3, doi:10.1002/andp.18892741206.

[38] A. Reuss, Berechnung der Fließgrenze von Mischkristallen auf Grund der Plastizitätsbedingung für Einkristalle ., ZAMM Journal of Applied Mathematics and Mechanics / Zeitschrift für Angewandte Mathematik und Mechanik 9 (1) (1929) 49–58. doi:10.1002/zamm.19290090104.

[39] Z. Hashin, S. Shtrikman, A variational approach to the theory of the elastic behaviour of multiphase materials, Journal of the Mechanics and Physics of Solids 11 (2) (1963) 127–140. doi:10.1016/0022-5096(63)90060-7.

[40] M. Chmielewski, W. Weglewski, Comparison of experimental and modelling results of thermal properties in Cu-AlN composite materials, Bulletin of the Polish Academy of Sciences: Technical Sciences 61 (2) (2013) 507–514. doi:10.2478/bpasts-2013-0050.

[41] J. D. Eshelby, The determination of the elastic field of an ellipsoidal inclution and related problems, Proceedings of the Physical Society of London, Series A 241 (1957) 376–396. doi:10.1098/rspa.1983.0054.

[42] T. Mori, K. Tanaka, Average stress in matrix and average elastic energy of materials with misfitting inclusions, Acta Metallurgica 21 (5) (1973) 571–574. doi:10.1016/0001-6160(73)90064-3.

[43] R. Hill, A self-consistent mechanics of composite materials, Journal of the Mechanics and Physics of Solids 13 (4) (1965) 213–222. doi:10.1016/0022-5096(65)90010-4.

[44] B. Budiansky, On the elastic moduli of some heterogeneous materials, Journal of the Mechanics and Physics of Solids 13 (4) (1965) 223–227. doi:10.1016/0022-5096(65)90011-6.

[45] G. Lielens, P. Pirotte, A. Couniot, F. Dupret, R. Keunings, Prediction of thermo-mechanical properties for compression moulded composites, Composites Part A: Applied Science and Manufacturing 29 (1-2) (1998) 63–70. doi:10.1016/S1359-835X(97)00039-0.

[46] R. A. Schapery, Thermal Expansion Coefficients of Composite Materials Based on Energy Principles, Journal of Composite Materials 2 (3) (1968) 380–404. doi:10.1177/002199836800200308.
URL http://journals.sagepub.com/doi/10.1177/002199836800200308

[47] N. J. Chamberlain, Derivation of Expansion Coefficients for a Fibre Reinforced Composites, Tech. rep., British Aircraft Corporation, London (1968).

[48] C. C. Chamis, Simplified composite micromechanics equations for hygral, thermal and mechanical properties, in: 38th Annual Conference of the Society of the Plastics Industry (SPI) Reinforced Plastics/Composites Institute, 1983.

[49] B. W. Rosen, Z. Hashin, Effective thermal expansion coefficients and specific heats of composite materials, International Journal of Engineering Science 8 (2) (1970) 157–173. doi:10.1016/0020-7225(70)90066-2.
URL http://linkinghub.elsevier.com/retrieve/pii/0020722570900662

[50] M. Sadd, Elasticity: Theory, Applications, and Numerics, Elsevier Science, 2014.
URL https://books.google.fr/books?id=-C-yNAEACAAJ

[51] S. Sihn, A. K. Roy, Micromechanical analysis for transverse thermal conductivity of composites, Journal of Composite Materials 45 (11) (2011) 1245–1255. doi:10.1177/0021998310382311.

[52] C. Karch, Micromechanical Analysis of Thermal Expansion Coefficients, Engineering Fracture Mechanics (July) (2014) 104–118. doi:10.4236/mnsms.2014.43012.

[53] D. E. Bowles, S. S. Tompkins, Prediction of Coefficients of Thermal Expansion for Unidirectional Composites, Journal of Composite Materials 23 (1989) 370–388.

[54] P. R. Evans, Rotations and rotation matrices, Acta Crystallographica - Section D Biological Crystallography 57 (10) (2001) 1355–1359. doi:10.1107/S0907444901012410.

[55] P. Vannucci, General anisotropic elasticity, in: Lecture Notes in Applied and Computational Mechanics, Vol. 85, 2018, pp. 19–73. doi:10.1007/978-981-10-5439-6_2.

[56] M. Ashby, E. Cope, D. Cebon, Materials Selection for Engineering Design, in: Informatics for Materials Science and Engineering, 2013, pp. 219–244. doi:10.1016/B978-0-12-394399-6.00010-2.
URL http://www.sciencedirect.com/science/article/pii/B9780123943996000102

[57] J. T. Mottram, B. Geary, R. Taylor, Thermal expansion of phenolic resin and phenolic-fibre composites, Journal of Materials Science 27 (18) (1992) 5015–5026. doi:10.1007/BF01105268.